



HAL
open science

Sampling and Meshing Submanifolds in High Dimension

Jean-Daniel Boissonnat, Siargey Kachanovich, Mathijs Wintraecken

► **To cite this version:**

Jean-Daniel Boissonnat, Siargey Kachanovich, Mathijs Wintraecken. Sampling and Meshing Submanifolds in High Dimension. 2019. hal-02386169v2

HAL Id: hal-02386169

<https://inria.hal.science/hal-02386169v2>

Preprint submitted on 29 Nov 2019

HAL is a multi-disciplinary open access archive for the deposit and dissemination of scientific research documents, whether they are published or not. The documents may come from teaching and research institutions in France or abroad, or from public or private research centers.

L'archive ouverte pluridisciplinaire **HAL**, est destinée au dépôt et à la diffusion de documents scientifiques de niveau recherche, publiés ou non, émanant des établissements d'enseignement et de recherche français ou étrangers, des laboratoires publics ou privés.

Sampling and Meshing Submanifolds in High Dimension

Jean-Daniel Boissonnat

Université Côte d’Azur, INRIA
[Sophia-Antipolis, France]
jean-daniel.boissonnat@inria.fr

Siargey Kachanovich

Université Côte d’Azur, INRIA
[Sophia-Antipolis, France]
siargey.kachanovich@inria.fr

Mathijs Wintraecken

IST Austria
[Klosterneuburg, Austria]
m.h.m.j.wintraecken@gmail.com

1 — Abstract —

2 This paper presents a rather simple tracing algorithm to sample and mesh an m -dimensional sub-
3 manifold of \mathbb{R}^d for arbitrary m and d . We extend the work of Dobkin et al. to submanifolds of
4 arbitrary dimension and codimension. The algorithm is practical and has been thoroughly invest-
5 igated from both theoretical and experimental perspectives. The paper provides a full description
6 and analysis of the data structure and of the tracing algorithm. The main contributions are :
7 1. We unify and complement the knowledge about Coxeter and Freudenthal-Kuhn triangulations.
8 2. We introduce an elegant and compact data structure to store Coxeter or Freudenthal-Kuhn
9 triangulations and describe output sensitive algorithms to compute faces and cofaces or any sim-
10 plex in the triangulation. 3. We present a manifold tracing algorithm based on the above data
11 structure. We provide a detailed complexity analysis along with experimental results that show
12 that the algorithm can handle cases that are far ahead of the state-of-the-art.

2012 ACM Subject Classification Theory of computation → Computational geometry

Keywords and phrases Coxeter triangulation, Kuhn triangulation, permutahedron, PL-approx-
imations, isomanifolds

Funding The research leading to these results has received funding from the European Research
Council (ERC) under the European Union’s Seventh Framework Programme (FP/2007-2013)
/ ERC Grant Agreement No. 339025 GUDHI (Algorithmic Foundations of Geometry Under-
standing in Higher Dimensions) and the European Union’s Horizon 2020 research and innovation
programme under the Marie Skłodowska-Curie grant agreement No. 754411.

Acknowledgements We thank Dominique Attali (CNRS), Arijit Ghosh (ISI), Vincent Pilaud
(École polytechnique), and Aurélien Alvarez (ENS Lyon) for their comments and suggestion. We
finally thank all former and current members of Datashape (formerly Geometrica) and Hebert
Edelsbrunner’s group for the stimulating environment in which the research was conducted.

Lines 500



© Jean-Daniel Boissonnat, Siargey Kachanovich, and Mathijs Wintraecken;
licensed under Creative Commons License CC-BY

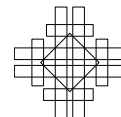
35th International Symposium on Computational Geometry (SoCG 2020).

Editors: ???; Article No. 00; pp. 00:1–00:23



Leibniz International Proceedings in Informatics

LIPIC Schloss Dagstuhl – Leibniz-Zentrum für Informatik, Dagstuhl Publishing, Germany



13 **1 Introduction**

14 This paper presents a rather simple algorithm to sample and mesh an m -dimensional sub-
 15 manifold of \mathbb{R}^d for arbitrary m and d . This fundamental problem finds applications in
 16 various fields like numerical analysis (to solve nonlinear differential equations) [3], dynam-
 17 ical systems (to approximate invariant manifolds) [39, 28]), chemistry (to study the energy
 18 landscape of molecules) [34], robotics (to describe the configuration space of mechanical sys-
 19 tems) [31], computer vision and graphics (to visualize time-varying and higher dimensional
 20 data) [5, 35].

21 **State-of-the-art.** The problem of triangulating differentiable manifolds has a long history
 22 in Mathematics dating back to the work of Cairns [12], Whitehead [44] and Whitney[45].
 23 More recently, the problem has received a lot of attention for surfaces of \mathbb{R}^3 in the Compu-
 24 tational Geometry and Computer Graphics communities. Among the widely used methods
 25 are the Marching cube algorithm [42] and Delaunay refinement [14]. In higher dimensions,
 26 some early work has been published in Applied Mathematics [1, 22, 39]. A slightly more
 27 recent paper by Dobkin et al. [21] attracted the interest of the Computer Graphics com-
 28 munity to Coxeter triangulations and their potential use for contour tracing. Although the
 29 authors only considered the case of curves ($m = 1$), it was claimed that the method could
 30 be “immediately generalized” to submanifolds of higher codimensions. However there has
 31 been only few works in that direction. This situation might be explained by the fact that
 32 extending the Marching cube algorithm to higher dimensions seems infeasible due to the
 33 large number of configurations that should be stored in a lookup table, and that no efficient
 34 data structure was known to store and query triangulations in high dimensions. The most
 35 recent work we are aware of is the work of Bhaniramka *et al.* [5] which is limited to hyper-
 36 surfaces ($m = d - 1$) and the work of Min [35]. Min’s method applies to submanifolds of
 37 any dimension and codimension. It uses an ambient triangulation instead of a cubical grid
 38 (the same Freudenthal-Kuhn triangulation used in this paper). However, in their analysis,
 39 they consider d as a constant and only report experimental results in dimensions 3 and 4.

40 The problem we consider is also related to the problem of *manifold reconstruction* from
 41 point samples [13, 7, 6]. A major difference however is that in manifold reconstruction, a
 42 sample is given as input while here we have to construct the sample using an oracle that
 43 queries the manifold. *Manifold sampling* is another related problem which is of fundamental
 44 algorithmic significance in statistics. Yet, not much is known beyond the convex case and
 45 the case of hypersurfaces ($m = d - 1$) [20, 36].

46 **Contributions.** This paper is the first of a series of related papers to fill the gap. In this
 47 paper, we extend the work of Dobkin et al. [21] to submanifolds of arbitrary codimension.
 48 The algorithm is practical and has been thoroughly investigated from theoretical and ex-
 49 perimental perspectives. This paper provides a full description and analysis of the data
 50 structure and of the tracing algorithm.

51 Guarantees on output of the the algorithm are established in two companion papers, one
 52 for the case of isomanifolds [10] and one for general smooth submanifolds [8]. Specifically, for
 53 isomanifolds we prove [10] that the output is a PL-manifold that has the same topology type
 54 as \mathcal{M} , and whose Fréchet distance to \mathcal{M} is small. Implementation details and experimental
 55 results will be discussed in [9]. The case of submanifolds with boundaries and, more generally,
 56 of stratified manifolds can be handled in very much the same way [9, 10].

57 The content of this paper is as follows. In Section 2, we first discuss Freudenthal-Kuhn
 58 and Coxeter triangulations, the latter exclusively of type \tilde{A}_d . These triangulations have
 59 different origins. Coxeter triangulations derive from geometric group theory, in particular

60 affine Weyl groups. Freudenthal-Kuhn triangulations are combinatorial by nature. Both
 61 triangulations are the same up to a linear transformation, as noted by [21] and fully proved
 62 in the appendix. This allows us to use on one hand the nice geometric properties of Coxeter
 63 triangulations of type \tilde{A}_d , where each simplex is very well shaped (large volume compared to
 64 longest edge length) and all simplices are identical up to reflections, and on the other hand
 65 the simple combinatorial definitions of the Freudenthal-Kuhn triangulation. Although most
 66 ideas in this section were known prior to this work, they were disseminated in many different
 67 areas and difficult to access. We elucidate those ideas, provide full proofs and combine them
 68 so as to extend them to arbitrary dimensions when necessary.

69 We then introduce a new data structure to compactly store Coxeter or Freudenthal-
 70 Kuhn triangulations. The data structure is an elegant and efficient representation of the
 71 combinatorial structure of those triangulations. We present a point location algorithm and
 72 describe output sensitive algorithms for computing faces and cofaces of simplices of all
 73 dimensions in the triangulation.

74 In Section 3, we present a submanifold tracing algorithm based on the above data struc-
 75 ture. The algorithm works for smooth submanifolds of any dimension and codimension.
 76 Starting from a given seed point, the algorithm probes the manifold using an oracle and
 77 outputs both a sample and a PL approximation of the manifold. A distinctive property
 78 of our algorithm, when compared to previous methods that work for submanifolds of ar-
 79 bitrary dimension and codimension [1, 35], is that its complexity depends mostly on the
 80 intrinsic dimension of the manifold (see Theorem 24 for a precise statement). Furthermore,
 81 using dimensionality reduction techniques, we can completely remove the dependency of
 82 the result on the ambient dimension (Theorem 26). The algorithm is quite simple and our
 83 implementation can handle cases that are far beyond what was possible before (Section 4).

84 **2 Coxeter-Freudenthal-Kuhn triangulations**

85 **2.1 Permutahedra**

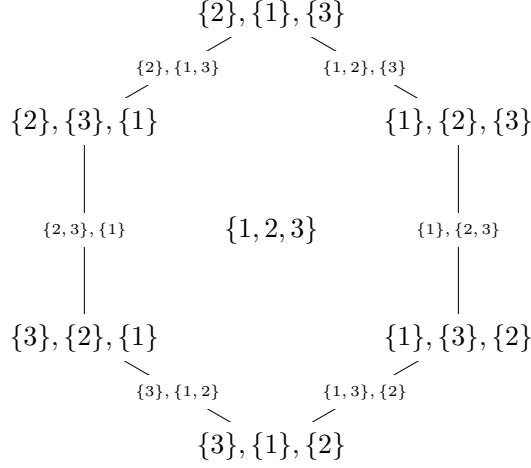
86 We write $[k] = \{1, \dots, k\}$ and $[k, l] = \{k, \dots, l\}$.

87 **► Definition 1 (Permutahedron).** A d -permutahedron is a d -dimensional polytope, which is
 88 the convex hull \mathcal{P} of all points in \mathbb{R}^{d+1} , the coordinates of which are permutations of $[d+1]$.
 89 Formally, this convex hull can be written as: $\mathcal{P} = \text{conv}\{(\sigma(1), \dots, \sigma(d+1)) \in \mathbb{R}^{d+1} \mid \sigma \in \mathfrak{S}_{d+1}\}$,
 90 where \mathfrak{S}_{d+1} denotes the set of permutations of $[d+1]$.

91 \mathcal{P} is at most d -dimensional since all its vertices lie on the hyperplane of equation
 92 $\sum_{i=1}^{d+1} x^i = \frac{d(d+1)}{2}$. Moreover, it can be shown that there are $d+1$ affinely independent
 93 vertices in \mathcal{P} , proving that \mathcal{P} is exactly d -dimensional (see for example [33, Lemma 3.4]).
 94 The facial structure of \mathcal{P} is best described in terms of ordered partitions [46].

95 **► Definition 2 (Ordered partition).** Let T be a finite non-empty set, $|T|$ its cardinality, and
 96 $l \leq |T|$ a positive integer. An *ordered partition* of T in l parts is an ordered collection of l
 97 subsets $\omega = (\omega_1, \dots, \omega_l)$, such that $\omega_i \subseteq T$ and $\{\omega_1, \dots, \omega_l\}$ is a partition of T . The ω_i
 98 are called the *parts*. We write $OP_l[d]$ for the set of ordered partitions of $[d]$ with l parts and
 99 just $OP[d]$ for the set of all ordered partitions of $[d]$.

100 **► Definition 3 (Refinement).** Let ω and ϖ be two ordered partitions of $[d+1]$ in k parts
 101 and l parts respectively, with $1 \leq k \leq l \leq d+1$. We say that ϖ is a *refinement* of
 102 ω if there exist positive integers a_1, \dots, a_k such that: $(\varpi_1, \dots, \varpi_{a_1})$ is an ordered parti-
 103 tion of ω_1 in a_1 parts, $(\varpi_{a_1+1}, \dots, \varpi_{a_1+a_2})$ is an ordered partition of ω_2 in a_2 parts, \dots ,
 104 $(\varpi_{a_1+\dots+a_{k-1}+1}, \dots, \varpi_{a_1+\dots+a_k})$ is an ordered partition of ω_k in a_k parts.



111 ■ **Figure 1** The 2-permutahedron and the ordered partitions associated to its faces.

105 ► **Lemma 4** (Facial structure of the permutahedron, Theorem 3.6 of [33]). *The faces of a d -*
 106 *permutahedron are in bijection with the ordered partitions of the set $[d + 1]$. More precisely,*
 107 *the l -faces of \mathcal{P} correspond to ordered partitions of $[d + 1]$ into $d + 1 - l$ parts $(\omega_1, \dots, \omega_{d+1-l})$*
 108 *such that all coordinates in ω_i are smaller than all coordinates in ω_j for $i < j$. If σ and*
 109 *τ are two faces of a d -permutahedron, σ is a subface of τ (noted $\sigma \subseteq \tau$) if and only if the*
 110 *ordered partition associated to σ is a refinement of the ordered partition associated to τ .*

112 ► **Corollary 5** (Corollary 3.15 of [33] and Theorem 3 of [37]). *The number of $(d - l)$ -dimensional*
 113 *faces in a d -permutahedron is $(l + 1)! S(d + 1, l + 1)$, where $S(\cdot, \cdot)$ is the Stirling number of*
 114 *the second kind. It is bounded by $2^{2(d+1) \log(l+1)}$.*

115 ► **Corollary 6.** *The number of vertices of a k -face of a d -permutahedron is at most $(k + 1)!$*

116 ► **Lemma 7.** *The number of facets of an l -face σ of a d -permutahedron is $O(2^l)$.*

117 Proofs of the previous two corollaries are added in Appendix B for completeness.

118 2.2 Freudhental-Kuhn triangulation

119 The Freudhental-Kuhn (FK for short) triangulation is obtained from the d -grid, i.e. the
 120 unit cubical tessellation of \mathbb{R}^d that consists of copies of the unit d -cube along the integer
 121 lattice \mathbb{Z}^d . By triangulating each d -cube in the grid in an appropriate way to be described
 122 now, we obtain the FK-triangulation of \mathbb{R}^d .

123 ► **Definition 8.** Let $x \in \mathbb{R}^d$ and write $z^i = x^i - \lfloor x^i \rfloor$. We denote by e_1, \dots, e_d the basis
 124 vectors and introduce, for reasons that will be clear later, the extra vector $e_{d+1} = -\sum_{i=1}^d e_i$.
 125 We introduce the convention that $z^{d+1} = 0$. We associate to x the ordered partition $\omega =$
 126 $(\omega_1, \dots, \omega_{l+1})$ of $[d + 1]$ where the ω_i are obtained by sorting the z^i in decreasing order.
 127 Specifically, with $\omega_i = \{\omega_i(1), \dots, \omega_i(m_i)\}$, we have

$$128 \quad 1 > z^{\omega_1(1)} = \dots = z^{\omega_1(m_1)} > \dots > z^{\omega_l(1)} = \dots = z^{\omega_l(m_l)} > z^{\omega_{l+1}(1)} = \dots = z^{\omega_{l+1}(m_{l+1})} = 0. \quad (1)$$

129 ► **Lemma 9.** *Suppose that $\omega = (\omega_1, \dots, \omega_{l+1})$ is an ordered partition of $[d + 1]$ and let*
 130 *$\sigma = \{v_0, \dots, v_l\}$ be the l -simplex whose vertices are the points*

$$131 \quad v_0 = (\lfloor x^1 \rfloor, \dots, \lfloor x^d \rfloor), \quad v_i = v_{i-1} + \sum_{i \in \omega_i} e_i \quad i = 1, \dots, l. \quad (2)$$

132 *Then x is a point in the relative interior of σ if and only if $z^i = x^i - \lfloor x^i \rfloor$, $i = 1, \dots, d + 1$*
 133 *(with, as above, $z^{d+1} = 0$ and $d + 1 \in \omega_{l+1}$), satisfy (1).*

134 **Proof.** Because the whole problem is translation invariant, we assume that $v_0 = 0$ without
 135 loss of generality, so that the expressions are shorter. Using barycentric coordinates, $z \in \sigma$
 136 can be written as

$$137 \quad z = \sum_{i=0}^l \lambda_i v_i = \sum_{i=0}^l \lambda_i \sum_{k=1}^i \sum_{j \in \omega_i} e_j$$

$$138 \quad = \lambda_l \left(\sum_{k \in \omega_l} e_k \right) + (\lambda_l + \lambda_{l-1}) \left(\sum_{k \in \omega_{l-1}} e_k \right) + \dots + (\lambda_l + \dots + \lambda_1) \left(\sum_{k \in \omega_1} e_k \right), \quad (3)$$

139 for some $\lambda_i > 0$ satisfying $\sum_{i=0}^l \lambda_i = 1$. We write

$$140 \quad \alpha_{\omega_l(1)} = \dots = \alpha_{\omega_l(m_l)} = \lambda_l$$

$$141 \quad \vdots$$

$$142 \quad \alpha_{\omega_1(1)} = \dots = \alpha_{\omega_1(m_1)} = \lambda_l + \dots + \lambda_1 \quad (4)$$

143 By construction $\alpha_{\omega_i(j)}$ is the $\omega_i(j)$ th coordinate of z , denoted by $z^{\omega_i(j)}$, while all coordinates
 144 $z^{\omega_{l+1}(1)}, \dots, z^{\omega_{l+1}(m_{l+1})}$ are zero, because $e_{\omega_{l+1}(i)}$ does not occur in (3), for all i . Moreover,
 145 because $\lambda_l + \dots + \lambda_i > \lambda_l + \dots + \lambda_{i-1}$, we see that (1) is satisfied.

146 Conversely, given a point z such that its coordinates satisfy (1), we can read of its
 147 barycentric coordinates with respect to the v_i , as defined by (2), from (4). ◀

148 ► **Theorem 10.** *The equivalence classes of the points of \mathbb{R}^d with a same ordered partition*
 149 *are the simplices of a triangulation of \mathbb{R}^d called the FK-triangulation.*

150 **Proof.** Lemma 9 implies that:

- 151 ■ Any face of a simplex in the FK-triangulation also lies in the FK-triangulation.
- 152 ■ The intersection of two simplices in the FK-triangulation also lie in the FK-triangulation.
- 153 ■ For any point $x \in \mathbb{R}^d$, there is a unique simplex σ such that x lies in the relative interior
 154 of σ . Because x has uniquely defined barycentric coordinates with respect to the vertices
 155 of σ it is mapped to a unique point in σ .

156 Hence the partition we have defined is a well-defined triangulation of \mathbb{R}^d . ◀

157 ► **Remark.** We note that, by construction, v_0 in Lemma 9 is the smallest vertex of σ in
 158 the lexicographical order. Lemma 9 also implies an observation of Freudenthal [25]: all
 159 d -simplices in the FK-triangulation can be described by monotone paths along the edges
 160 of the cube from vertex $(0, \dots, 0) + v_0$ to vertex $(1, \dots, 1) + v_0$. Conversely, any monotone
 161 path along the edges of the cubes from $(0, \dots, 0) + v_0$ to $(1, \dots, 1) + v_0$ gives a simplex in
 162 the FK-triangulation.

163 **Cycles and the permutahedron.** This monotone path can be made into a cycle using the
 164 extra vector e_{d+1} , introduced by Eaves [22], because by construction $v_0 = v_l + \sum_{i \in \omega_{l+1}} e_i$,
 165 with ω as in Definition 8. Because it is a cycle, we can take any vertex of the cycle as a
 166 starting point, which means that v_0 no longer has a special role as a starting point of a
 167 monotone edge walk. A cycle can now be represented by an ordered partition of $[d+1]$, for
 168 which it is not longer necessary that $d+1$ lies in ω_{l+1} , and an (arbitrary) starting point.

169 We now formalize these general cyclical paths:

170 ► **Definition 11** (Permutahedral representation). Let $(v_0, \omega) \in \mathbb{Z}^d \times OP_{l+1}[d]$. To this pair
 171 we associate a simplex $\sigma^\omega = \{v_0 = v_0^\omega, v_1^\omega, \dots, v_l^\omega\}$ with

$$172 \quad v_i^\omega = v_{i-1}^\omega + \sum_{i \in \omega_i} e_i \quad i = 1, \dots, l. \quad (5)$$

173 We say that (v_0, ω) is the permutahedral representation of the simplex σ^ω . If $d+1 \in \omega_{l+1}$
 174 we say that (v_0, ω) is the canonical permutahedral representation of σ^ω . In this case, σ^ω is a
 175 simplex in the FK-triangulation in the cube of which v_0 is the minimal vertex with respect
 176 to the lexicographical order, as we have seen above. In Lemma 14 and Proposition 15 we'll
 177 see that, more generally, $\{(v_0, \omega) \mid \omega \in OP[d+1]\}$ is the star of v_0 in the FK-triangulation,
 178 where we identify simplices with their permutahedral representations.

179 ► **Definition 12** (Cyclic shifts). Let (v_0, ω) be a permutahedral representation. We define
 180 the cyclic shift of (v_0, ω) of length k to the left as (v'_0, ω') , where

$$181 \quad v'_0 = v_0 + \sum_{j=1}^k \sum_{i \in \omega_j} e_i \quad \omega'_j = \omega_{(j+k-1) \bmod (l+1)+1}. \quad (6)$$

182 Here we use the convention that the sum from 1 to 0 is empty. We write $(v'_0, \omega') = (v_0, \omega) \oplus k$.

183 ► **Lemma 13.** *The cyclic shift $(v'_0, \omega') = (v_0, \omega) \oplus k$ defines the same simplex as (v_0, ω) .*

184 **Proof.** Follows by inserting (6) in (5). ◀

185 We now prove that the all permutahedral representations for a fixed v_0 , form the star of
 186 v_0 . This is a crucial property that will be used to efficiently compute faces and cofaces and
 187 traverse the triangulation.

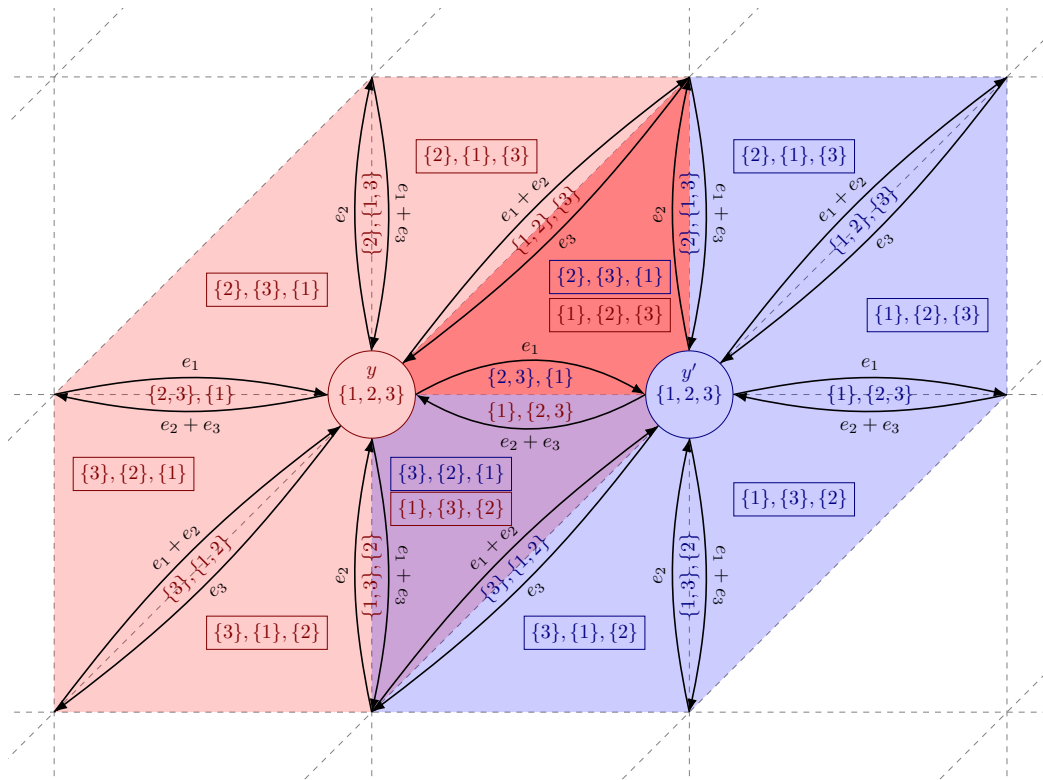
188 ► **Lemma 14.** *The set $\{(v_0, \omega) \mid \omega \in OP[d+1]\}$, where $OP[d+1]$ is the set of all ordered
 189 partitions of $[d+1]$, gives all the simplices in the star of v_0 in FK-triangulation.*

190 **Proof.** Let (v_0, ω) , with $\omega \in OP_{l+1}[d+1]$, be such that $d+1 \in \omega_k$. Let $(v'_0, \omega') = (v_0, \omega) \oplus$
 191 $(l-k+1)$. By Definition 12 and Lemma 13, (v_0, ω) and (v'_0, ω') represent the same simplex.
 192 Moreover $d+1 \in \omega'_{l+1}$, that is (v'_0, ω') is a canonical permutahedral representation. This
 193 implies that (v'_0, ω') lies in the FK-triangulation by Lemma 9 and Theorem 10.

194 Conversely, suppose that (v'_0, ω') is the canonical permutahedral representation of a
 195 simplex in the star of v_0 , that is there is some k such that $v'_k = v_0$, with v'_k as in (2). Then
 196 $(v_0, \omega) = (v'_0, \omega') \oplus k$ is also a permutahedral representation of the same simplex. ◀

197 **Faces.** From (5) it is clear that merging two consecutive parts in the ordered partition
 198 $\omega = (\omega_1, \dots, \omega_{l+1})$ corresponds to removing a vertex from the simplex, that is taking a
 199 facet. Here we stress that we allow to merge ω_1 , and ω_{l+1} , but in that case we have to
 200 change the base point of the cycle to $v_0 + \sum_{i \in \omega_1} e_i$. For example, when looking at the two
 201 dimensional example in Figure 2, we see that the edges that contain y in the red triangle with

202 permutahedral representation $(y, (\{1\}, \{2\}, \{3\}))$ are $(y, (\{1, 2\}, \{3\}))$, and $(y, (\{1\}, \{2, 3\}))$.
 203 The third edge of the red triangle is $(y', (\{2\}, \{1, 3\}))$. Generally, given an ordered partition
 204 ω in $l+1$ parts all $(l-j)$ -faces can be found by merging j consecutive parts in ω (for example
 205 merging ω_1 with ω_2 and ω_3 with ω_4), where we allow ω_{l+1} to merge with ω_1 , but in this
 206 case we again need to change the base point.



207 ■ **Figure 2** The permutahedral representation of the simplices in the stars of vertices y and y' .

208 Because the combinatorial structure of the faces is compatible with the permutahedron,
 209 Lemma 14 immediately gives:

210 ► **Proposition 15.** *The star of v_0 is dual to a permutahedron (combinatorially).*

211 This proposition also explains the nomenclature permutahedral representation.

212 2.3 Basic operations

213 **Point location** Given a point $x \in \mathbb{R}^d$ Lemma 9 tells us how to find the canonical permutahedral
 214 representation of the simplex in which x is contained. The complexity of point
 215 location is dominated by the sorting of the $z^i = x^i - \lfloor x^i \rfloor$, which takes $O(d \log d)$ time and
 216 requires $O(d)$ space.

217 **Face computation.** Let σ be an l -simplex whose canonical permutahedral representation
 218 is (v_0, ω) , where ω is an ordered partition of $[d+1]$ into $l+1$ parts. The computation of all
 219 k -faces of σ goes as follows. We use Ehrlich's subset generation algorithm [24] to compute

220 all the subsets of $k + 1$ elements from $\{v_0, \dots, v_l\}$. Let $\tau = \{v_{m_0}, \dots, v_{m_k}\}$ be such a subset.
 221 τ is a k -face of σ . We then compute the canonical permutahedral representation of all those
 222 k -faces τ .

223 We first sort the m_i so that $m_0 < \dots < m_k$ using counting sort. Then, the canonical
 224 permutahedral representation (\tilde{v}'_0, ω') of τ is found by merging consecutive parts of ω so as
 225 to obtain $k + 1$ parts as follows :

$$226 \quad v'_0 = v_{m_0} = v_0 + \sum_{j \in \omega_1} e_j + \dots + \sum_{j \in \omega_{m_0-1}} e_j$$

$$227 \quad \omega'_i = \omega_{m_{i-1}} \cup \dots \cup \omega_{m_i-1} \quad \text{for } i \in \{1, \dots, k\}$$

$$228 \quad \omega'_{k+1} = (\omega_1 \cup \dots \cup \omega_{m_0-1}) \cup (\omega_{m_k} \cup \dots \cup \omega_{l+1}).$$

229 The complexity of computing all subsets of $k + 1$ vertices of σ using Ehrlich's algorithm
 230 takes time $O(k + s)$ where $s = \binom{l+1}{k+1}$ is the number of subsets. Computing, for each such
 231 k -simplex its permutahedral representation takes $O(d)$ time.

232 ► **Lemma 16.** *Let σ be an l -simplex in the FK-triangulation of \mathbb{R}^d given by its canonical*
 233 *permutahedral representation. Computing the canonical permutahedral representations of*
 234 *all its k -faces can be done in time $O(ds)$, where $s = \binom{l+1}{k+1}$ is the number of k -faces of an l*
 235 *simplex. The space complexity of the algorithm is $O(l)$ from the counting sort.*

236 **Coface computation.** Computing the faces of a simplex σ consisted in coarsifying its
 237 ordered partition. The computation of cofaces is the reverse. Here we refine the ordered
 238 partition. Specifically, if σ is a k -simplex represented by its canonical permutahedral repres-
 239 entation (v_0, ω) , and we want to compute its l -cofaces, we need to compute all refinements
 240 of ω into $l + 1$ parts.

241 More precisely, we need to subdivide each ω_i in $a_i \leq |\omega_i|$ subparts so that $\sum_{i=1}^{k+1} a_i = l + 1$.
 242 This can be done in time proportional to the number $k + 1$ of the generated subparts. We
 243 then need to consider all the permutations of these subparts since we are interested in
 244 ordered partitions. Using known algorithms by Walsh [41] and Ruskey and Savage [38], we
 245 can compute all the ordered partitions associated to the l -cofaces of σ in time proportional
 246 to the number of such cofaces. We thus obtain all the permutahedral representations (v_0, ω')
 247 of all the l -cofaces of σ .

248 It is important to notice that all cofaces of σ have v_0 as a vertex. However v_0 is not
 249 necessarily the minimal vertex of some of the computed cofaces. We thus have to identify
 250 the minimal vertex of each computed coface and use cyclic shifts as in Lemma 14 to obtain
 251 the canonical permutahedral representation of the coface.

252 ► **Lemma 17.** *Let σ be a k -simplex in the FK-triangulation of \mathbb{R}^d given by its permutahedral*
 253 *representation. Computing the permutahedral representations of all its l -cofaces can be done*
 254 *in time $O(ds)$, where s is the number of l -cofaces of a k -simplex in the FK-triangulation.*
 255 *The space complexity of the algorithm is $O(d)$.*

256 2.4 Coxeter triangulations of type \tilde{A}_d

257 The Freudenthal-Kuhn triangulation is closely related to the Coxeter triangulation [18] of
 258 type \tilde{A}_d . There are many equivalent ways to define the Coxeter triangulation of type \tilde{A}_d ,
 259 see [11, 15, 29]. We recall the following:

260 ▶ **Definition 18.** Let $P = \{(x^i) \in \mathbb{R}^{d+1} \mid \sum_i x^i = 0\}$ and consider the d -simplex with
 261 vertices u_k in P .

$$262 \quad u_0 = \left(0^{\{d+1\}}\right) \quad u_k = \left(\left(-\frac{d+1-k}{d+1}\right)^{\{k\}}, \left(\frac{k}{d+1}\right)^{\{d+1-k\}}\right), \quad k \in [d],$$

263 where $x^{\{k\}}$ denotes k consecutive coordinates x . The Coxeter triangulation of type \tilde{A}_d in P
 264 is found by consecutively reflecting the simplex in its faces.

265 The following lemma relates Coxeter and FK-triangulations and was first stated in [21].

266 ▶ **Lemma 19.** *The Freudenthal-Kuhn triangulation and Coxeter triangulation of type \tilde{A}_d*
 267 *are identical up to a linear transformation.*

268 A proof can be found in Appendix A. We will now call any triangulation of Euclidean space
 269 that is the image of a Coxeter triangulation under a non-degenerate affine map a Coxeter-
 270 Freudenthal-Kuhn triangulation, or CFK-triangulation for short. Moreover, we have

271 ▶ **Lemma 20** ([15]). *The Coxeter triangulation of type \tilde{A}_d is a Delaunay triangulation.*

272 We note that Proposition 15, together with Lemmas 19 and 20, give an alternative self-
 273 contained proof of the known fact [17, Chapter 21, Section 3.F] (also proved in Appendix A
 274 for completeness) that the Voronoi cell of a vertex in \tilde{A}_d is a (combinatorial) permutahedron.

275 The simplices in the Coxeter triangulation of type \tilde{A}_d have extremely good quality [15].
 276 For example, the volume compared to the longest edge length to the d -th power is large. As
 277 we will see, the exceptional quality of Coxeter improves the running of our algorithms.

278 2.5 Data structure for storing CFK-triangulations

279 To store an ambient CFK-triangulation for the manifold tracing algorithm in Section 3,
 280 we use the following data structure. This data structure contains information on both the
 281 combinatorial structure and the geometry of the triangulation. The combinatorics of the
 282 triangulation is given through the canonical permutahedral representation of its simplices
 283 and the algorithms from Section 2.2. The geometry of the triangulation is specified by the
 284 affine transformation that maps the FK-triangulation of \mathbb{R}^d to the CFK-triangulation. The
 285 affine transformation is given by a $d \times d$ matrix Λ and a d -vector b .

286 ▶ **Remark.** Matrix Λ is used to compute the coordinates of the vertices of simplices and, for
 287 the most useful cases in practice, needs not to be explicitly stored. For the FK-triangulation,
 288 Λ is the identity matrix and $b = 0$, therefore no storage is required. For the Coxeter
 289 triangulation of type \tilde{A}_d , we can directly access the coordinates of vertices as given in
 290 Definition 18.

291 3 Sampling and meshing submanifolds

292 In this section, we describe an algorithm that will compute a PL-approximation of an m -
 293 submanifold of \mathbb{R}^d for arbitrary d and $m \leq d$. The algorithm can be considered as an
 294 alternative to the Marching Cube algorithm [32] where the usual cubical grid is replaced by a
 295 CFK — preferably the Coxeter — triangulation of the ambient space. Taking a triangulation
 296 instead of a grid is a major advantage in high dimensions that has been recognized in the
 297 pioneering works of Allgower and Schmidt [2] and of Dobkin et al. [21]. See also [35]. By
 298 taking as a triangulation of the ambient space a CFK-triangulation, we keep two main
 299 advantages of using grids: very limited storage and fast basic operations.

321 **Algorithm 1** Manifold tracing algorithm

321 **input** : Triangulation \mathcal{T} of \mathbb{R}^d , manifold \mathcal{M} of dimension m , seed point $x_0 \in \mathcal{M}$
322 **output**: Set \mathcal{S} of the simplices in \mathcal{T} of dimension $k = d - m$ that intersect \mathcal{M}
323 Translate \mathcal{T} so that x_0 coincides with the barycentre of a k -dimensional face τ_0 in \mathcal{T}
324 Initialize the queue \mathcal{Q} and the set \mathcal{S} with τ_0
325 **while** the queue \mathcal{Q} is not empty **do**
326 Pop a k -dimensional simplex τ from \mathcal{Q}
327 **foreach** cofacet ϕ of τ **do**
328 **foreach** facet ρ of ϕ **do**
329 **if** ρ does not lie in \mathcal{S} and intersects \mathcal{M} **then**
330 Insert ρ to the queue \mathcal{Q}
331 Insert ρ together with the intersection point to the output set \mathcal{S}

300 3.1 Manifold tracing algorithm

301 Let \mathcal{M} be an m -dimensional compact submanifold of the Euclidean space \mathbb{R}^d . Both m
302 and d are known but arbitrary and will be considered as parameters in the complexity
303 analysis. The algorithm will use a CFK-triangulation \mathcal{T} of \mathbb{R}^d , which is stored using the
304 data structure from Section 2.5. We assume that the manifold \mathcal{M} and the triangulation \mathcal{T}
305 satisfy a genericity hypothesis:

306 **► Hypothesis 21 (Genericity).** *The manifold has an empty intersection with all simplices of*
307 *dimensions strictly lower than k in the triangulation \mathcal{T} . The intersection of the manifold*
308 *\mathcal{M} and any k -dimensional simplex in the triangulation \mathcal{T} is a single point.*

309 **► Remark.** It turns out [10] that for an isomanifold $f^{-1}(0)$ it suffices to find the intersection
310 points of $f_{\text{PL}}^{-1}(0)$ with the k -simplices under very weak conditions. Here f_{PL} denotes the
311 function that is linear on every simplex in \mathcal{T} and coincides with f on the vertices of \mathcal{T} . We
312 stress that $f_{\text{PL}}^{-1}(0)$ satisfies the genericity hypothesis with probability one.

313 We assume that we know a point on the manifold $x_0 \in \mathcal{M}$, from which the algorithm
314 starts. If \mathcal{M} consists of multiple connected components, then a seed point per each connected
315 component must be provided and we proceed in the same manner for each component. So
316 we will assume for now that \mathcal{M} is connected.

317 In addition, we assume that the manifold \mathcal{M} can be accessed through an *oracle* that
318 allows us to answer whether a k -simplex in the triangulation \mathcal{T} intersects the manifold \mathcal{M} .
319 Here, $k = d - m$ is the codimension of \mathcal{M} . In the following, we will refer to this oracle as
320 the *intersection oracle*.

322 The algorithm is described as Algorithm 1. We first translate the coordinate frame so
323 that x_0 is the barycenter of a k -simplex of \mathcal{T} (any such simplex is fine). This simplex is put
324 in the set \mathcal{S} of the simplices in \mathcal{T} of dimension $k = d - m$ that intersect \mathcal{M} . Then, given such
325 a simplex, we look at all its cofacets that have not been considered yet and consider all the
326 facets of those cofacets that have not been considered yet. This can be done using a queue
327 \mathcal{Q} of simplices to consider. Each of these simplices is queried with the intersection oracle
328 and, if it is found to intersect \mathcal{M} , it is added to \mathcal{S} . Upon termination, \mathcal{S} contains all the
329 k -dimensional simplices of \mathcal{T} that intersect \mathcal{M} . Since, by our genericity assumption, each
330 k -simplex in \mathcal{S} intersects \mathcal{M} in a single point, $|\mathcal{S}|$ is also the size of the sample produced by
331 our algorithm. A better approximation of the sample is of course possible if we have at our

332 disposal a more powerful intersection oracle that not only detects intersections but can also
 333 compute intersection points between the simplices in \mathcal{S} and \mathcal{M} .

334 A polyhedron can be deduced from \mathcal{S} by taking the dual faces of the simplices in \mathcal{S} . A
 335 more precise approximation can be obtained if, in addition to the intersection oracle, we
 336 can also compute the intersection points $\mathcal{S} \cap \mathcal{M}$. This will be described in full detail in a
 337 companion paper.

338 3.2 Complexity analysis

339 We can easily bound the complexity of the manifold tracing algorithm as a function of the
 340 size of the output.

341 ► **Proposition 22.** *The time complexity of the algorithm is $O(k2^m I |\mathcal{S}|)$. where I is the time
 342 complexity of one call of the intersection oracle and $|\mathcal{S}|$ is the size of the output.*

343 **Proof.** The complexity of the initialization is $O(d)$. The complexity of each iteration of
 344 the while loop consists of: computing the cofacets of the popped k -dimensional simplex in
 345 the queue, computing facets of these cofacets and applying the intersection oracle on each
 346 of these facets. From Lemma 7, the number of cofacets is $O(2^m)$. Each of these cofacets
 347 has $k + 2$ facets. Therefore, for each iteration of the while loop, the algorithm applies the
 348 intersection oracle on $O(k2^m)$ simplices. By using this observation and the complexities in
 349 Lemmas 16 and 17, the total time complexity of each iteration of the while loop follows:

$$350 \quad O(d2^m) + O(dk2^m) + O(k2^m I) = O(k2^m(d + I)) = O(k2^m I).$$

351 Since there are $|\mathcal{S}|$ iterations of the while loop, the result follows. ◀

352 We will now express the size of the output in terms of quantities that depend on the
 353 manifold and the resolution of the triangulation.

► **Proposition 23** (Size of the output).

$$354 \quad |\mathcal{S}| \leq \frac{C}{\Theta \sqrt{m}} \left(\frac{2\pi e}{k}\right)^{k/2} \left(\frac{2}{\delta}\right)^m \text{vol}_m(\mathcal{M}) = O\left(2^{O(d \log d)} \frac{\text{vol}_m(\mathcal{M})}{\delta^m}\right).$$

355 where:

- 356 ■ $\text{vol}_m(\mathcal{M})$ is the m -dimensional volume of \mathcal{M} ,
- 357 ■ δ is the diameter of the d -simplices of \mathcal{T} and a measure of the resolution of \mathcal{T} ,
- 358 ■ V is the volume of any d -simplex of \mathcal{T} , and $\Theta = \frac{V}{\delta^d}$ its fatness,
- 359 ■ C is a constant that does not depend on d , m or δ .

360 **Proof.** Let \mathcal{N} be the set of the d -dimensional cofaces of the simplices in \mathcal{S} , and let N be
 361 the cardinality of \mathcal{N} . In the proof we will use constants C_1, C_2, C_3 that are constants that
 362 do not depend on d , m nor δ .

363 **Upper bound on N .** Write \mathcal{M}^δ for the tubular neighbourhood of \mathcal{M} of radius δ , i.e. the
 364 set of points at distance at most δ from \mathcal{M} . Since the d -dimensional simplices in \mathcal{N} have
 365 pairwise disjoint interiors and all lie inside \mathcal{M}^δ , we have

$$366 \quad N \cdot V \leq \text{vol}_d(\mathcal{M}^\delta). \tag{7}$$

00:12 Sampling and Meshing Submanifolds

367 According to the tube formula of Weyl [43, 26] and writing B_k for the volume of the unit
368 ball of dimension k , there exists constants C_1 and C_2 such that

$$369 \quad \text{vol}_d(\mathcal{M}^\delta) \leq C_1 B_k \delta^k \text{vol}_m(\mathcal{M}) \leq C_2 \left(\frac{2\pi e}{k}\right)^{k/2} \delta^k \text{vol}_m(\mathcal{M}) \quad (8)$$

370 By combining the two inequalities (7) and (8), we get:

$$371 \quad N \leq \frac{\text{vol}_d(\mathcal{M}^\delta)}{V} \leq C_2 \left(\frac{2\pi e}{k}\right)^{k/2} \frac{\delta^k}{V} \text{vol}_m(\mathcal{M}) \leq C_2 \left(\frac{2\pi e}{k}\right)^{k/2} \frac{1}{\Theta} \frac{\text{vol}_m(\mathcal{M})}{\delta^m}. \quad (9)$$

372 where Θ is the fatness of the simplices in the triangulation \mathcal{T} . Note that the dependency of
373 N on $1/\delta$ is exponential in m but not in d .

374 **Upper bound on $|\mathcal{S}|$.** Now, we express $|\mathcal{S}|$ in terms of N , d and m . For this, we count
375 the number INC of incidences of the k -dimensional simplices in \mathcal{S} and the d -dimensional
376 simplices in \mathcal{N} in two ways:

$$377 \quad \sum_{\tau \in \mathcal{S}} |\text{cof}(\tau, d)| = \text{INC} = \sum_{\sigma \in \mathcal{N}} |\text{fac}(\sigma, k) \cap \mathcal{S}|. \quad (10)$$

378 The number of d -cofaces of a k -simplex is given by Corollary 6 applied to the dual Voronoi
379 face of τ . Hence there exists a constant C_3 such that for any k -dimensional simplex $\tau \in \mathcal{S}$,
380 we have:

$$381 \quad |\text{cof}(\tau, d)| \geq C_3 \left(\frac{d}{m+1}\right)^{m+1}.$$

382 On the other hand, for each d -dimensional simplex $\sigma \in \mathcal{N}$, we have :

$$383 \quad |\text{fac}(\sigma, k) \cap \mathcal{S}| \leq |\text{fac}(\sigma, k)| = \binom{d+1}{m+1}.$$

384 Equation (10) becomes

$$385 \quad C_3 \left(\frac{d}{m+1}\right)^{m+1} |\mathcal{S}| \leq \sum_{\tau \in \mathcal{S}} |\text{cof}(\tau, d)| = \sum_{\sigma \in \mathcal{N}} |\text{fac}(\sigma, d) \cap \mathcal{S}| \leq \binom{d+1}{m+1} N,$$

386 from which we get using (9) that there exists a constant C such that

$$387 \quad |\mathcal{S}| \leq C \left(\frac{2\pi e}{k}\right)^{k/2} \frac{1}{\Theta} \text{vol}_m(\mathcal{M}) m^{-1/2} (2/\delta)^m.$$

388 **Bound on fatness.** The fatness term Θ in the expression in Proposition 23 depends on
389 the choice of the triangulation \mathcal{T} . The fatness Θ_{CT} of the d -dimensional simplices in the
390 Coxeter triangulation is given by (see [15])

$$391 \quad \frac{1}{\Theta_{CT}} = O\left(\frac{d^{(d+1)/2} d!}{2^d}\right) = O(2^{O(d \log d)}). \quad (11)$$

392 while the fatness Θ_{FKT} of the d -dimensional simplices in the FK-triangulation of \mathbb{R}^d is given
393 by (see [19])

$$394 \quad \frac{1}{\Theta_{FKT}} = O\left(d^{d/2} d!\right) = O(2^{O(d \log d)}). \quad (12)$$

395 Note that, in both cases, Θ depends on the ambient dimension but not on δ . Note also
 396 that, while similar, the two bounds on the fatness differ by a factor $2^d/\sqrt{d}$. We thus expect
 397 that using the Coxeter triangulation as the ambient triangulation will give a smaller output
 398 \mathcal{S} than the one we obtain using the Freudenthal-Kuhn triangulation. This is confirmed in
 399 practice as shown in Section 4 (see Figure 6). ◀

400 We combine Propositions 22 and 23 in the following theorem.

401 ▶ **Theorem 24.** *The time complexity of the manifold tracing algorithm is $2^{O(d \log d)} I \frac{\text{vol}_m(\mathcal{M})}{\delta^m}$,*
 402 *where I is the time complexity of one call of the intersection oracle.*

403 **Cost of the oracle.** The cost of I depends on how the submanifold is given. As an example,
 404 consider the case where \mathcal{M} is the PL-approximation of the zero set of a function $f : \mathbb{R}^d \rightarrow \mathbb{R}^k$
 405 and assume that evaluating f at any point $x \in \mathbb{R}^d$ can be done in time polynomial in d
 406 (which, in particular, is true if each f^i is a polynomial in the coordinates of x). Then I
 407 depends polynomially on d too. Indeed, consider a k -simplex σ of the triangulation on which
 408 we call the intersection oracle and let H denote the m -flat that linearly interpolates $f^{-1}(0)$
 409 inside σ . To implement the oracle, we first evaluate f at the vertices of σ . We then compute
 410 the barycentric coordinates of the (generically unique) point of intersection of the affine hull
 411 of σ with H . Lastly, we check whether the barycentric coordinates are all non-negative (to
 412 ensure that the intersection point lies inside σ). It follows that the cost of the oracle is the
 413 cost of evaluating f at the $k + 1$ vertices of σ plus the cost of solving a linear system of k
 414 equations and k unknowns, which can be done in time $O(k^{2.375})$.

415 **Dimensionality reduction.** As seen from Proposition 23, the size \mathcal{S} of the output of
 416 the algorithm, considered as a function of the resolution $1/\delta$ of the triangulation, depends
 417 exponentially on m (which is to be expected) and not on d (which is fortunate). Nevertheless,
 418 the size of the output depends exponentially on d . This, in particular, means that the sample
 419 constructed by the algorithm, although δ -dense, is not guaranteed to be $\mu\delta$ separated for
 420 some constant μ . In other words, the output sample is not a net of the manifold.

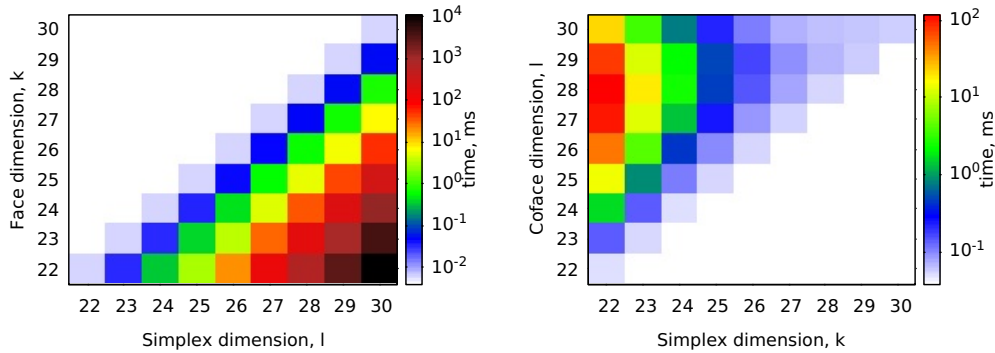
421 We can improve on the bound on \mathcal{S} by using dimensionality reduction techniques and,
 422 specifically, a variant of the celebrated Johnson-Lindenstrauss lemma for manifolds. We
 423 depart from our previous worst-case analysis by allowing some approximation factor ε and
 424 tolerate a guarantee that holds only with high probability.

425 ▶ **Theorem 25** (Johnson-Lindenstrauss lemma for manifolds [16, 40])). *Pick any $\varepsilon, \eta > 0$,*
 426 *and let $d' = \Omega\left(\frac{m}{\varepsilon^2} \log \frac{1}{\varepsilon} + \frac{1}{\varepsilon^2} \log \frac{\Gamma}{\delta}\right)$, where Γ is a quantity that depends only on intrinsic*
 427 *properties of \mathcal{M} . Let Φ be a random affine subspace of dimension d' . Then, with probability*
 428 *$> 1 - \eta$, for all $x, y \in \mathcal{M}$*

429
$$(1 - \varepsilon) \sqrt{\frac{d'}{d}} \leq \frac{\|\Phi x - \Phi y\|}{\|x - y\|} \leq (1 + \varepsilon) \sqrt{\frac{d'}{d}}.$$

430 It follows that the image $\Phi\mathcal{M}$ of \mathcal{M} will be a submanifold of dimension m embedded in
 431 $\mathbb{R}^{d'}$. One can now run the manifold tracing algorithm in $\mathbb{R}^{d'}$ to sample and mesh $\Phi\mathcal{M}$.
 432 The algorithm works as described before except that we need another oracle that, given a
 433 $(d' - m)$ -simplex σ of the CFK-triangulation of $\mathbb{R}^{d'}$, decides whether its inverse image $\Phi^{-1}\sigma$,
 434 which is a $(d - d')$ -dimensional flat strip in \mathbb{R}^d , intersects \mathcal{M} or not.

435 Due to the scaling factor $\sqrt{d/d'}$, the resolution of the triangulation in the low dimensional
 436 plane has to be scaled by the same factor if one wants to satisfy a given sampling density
 437 on \mathcal{M} . Since the geometry of the manifold (reach and volume) is also scaled in the same
 438 way [23], the analysis of the algorithm will be unchanged. Theorem 24 shows that the



455 **Figure 3** On the left: comparison of the execution time of the face and the coface generation
 456 algorithm for simplices of various dimensions in a CFK-triangulation of \mathbb{R}^{30} . Because the average
 457 computation time of a face or coface is constant, the presented time is proportional to the number of
 458 faces or cofaces of respective simplices.

439 output sample will have size $O\left(2^{O(d' \log d')} \frac{\text{vol}_m(\mathcal{M})}{\delta^m}\right)$. Since d' does not depend on the
 440 ambient dimension d by Theorem 25, neither does the size of the output sample.

441 **► Theorem 26.** *Pick any $\varepsilon, \eta > 0$, and let $d' = \Omega\left(\frac{m}{\varepsilon^2} \log \frac{1}{\varepsilon} + \frac{1}{\varepsilon^2} \log \frac{\Gamma}{\delta}\right)$, where Γ is a
 442 quantity that depends only on intrinsic properties of \mathcal{M} . Let Φ be a random affine subspace
 443 of dimension d' . Then, with probability $> 1 - \eta$, we can sample and mesh \mathcal{M} using the tracing
 444 algorithm in $\mathbb{R}^{d'}$ and the new oracle. The size of the output is $O\left(2^{O(d' \log d')} \frac{\text{vol}_m(\mathcal{M})}{\delta^m}\right)$.*

445 The previous theorem bounds the size of the output. The complexity of the new oracle
 446 is the same as the complexity of the basic intersection oracle.

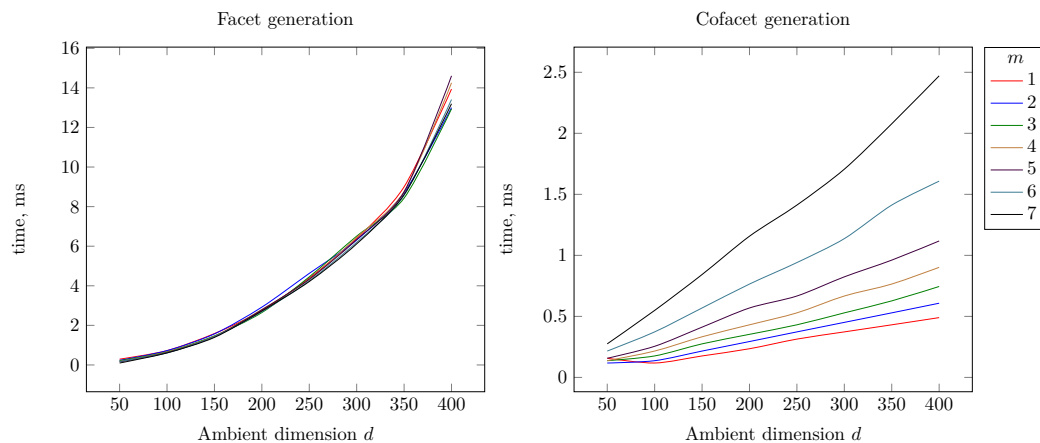
447 4 Experimental results

448 The data structure of Section 2 and the algorithm of Section 3 have been implemented in
 449 C++. The code is robust and fast, and will be released soon in the GUDHI library [27]. Full
 450 detail on the implementation, including the implementation of the oracle, will be reported
 451 in a companion paper together with experimental results [9]. See also [30].

452 In this section, we explore the dependency of our C++ implementation of the data struc-
 453 ture for the ambient CFK-triangulation and of the manifold tracing algorithm on the prop-
 454 erties of the triangulation and of the input manifold.

461 Data structure.

462 In Figure 3, we present the time of generating all faces (on the left) and all cofaces (on the
 463 right) of various dimensions of simplices in a CFK-triangulation of \mathbb{R}^{30} using algorithms
 464 from Section 2.2. The presented execution time is averaged over 500 tests. Note that both
 465 for face and coface generation algorithms, the execution time is proportional to the number
 466 of computed elements. On average, these algorithms take time 0.001-0.002 ms per computed
 467 face or coface, regardless of the dimensions of the input simplex and of the computed element.
 468 In Figure 4, we further illustrate the particular case of facet and cofacet computation, which
 469 is essential in the manifold tracing algorithm. We show the dependency of the execution
 470 time on two parameters: the ambient dimension d and the codimension m of the input

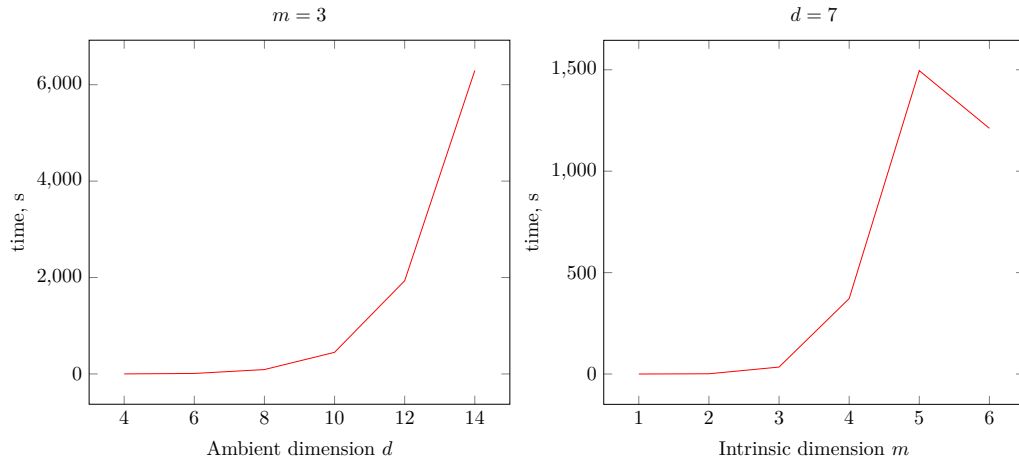


459 **Figure 4** Execution time of the facet and cofacet computation depending on the dimension d of
 460 the triangulation and the codimension m of the input simplex.

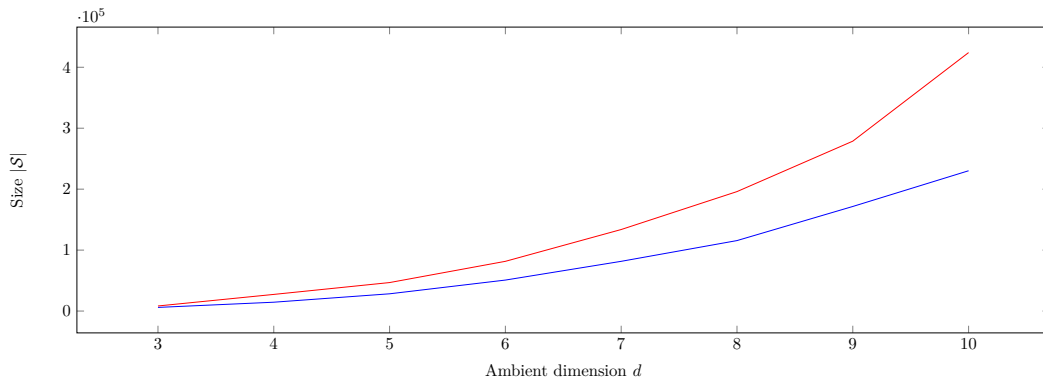
471 simplex, which corresponds to the intrinsic dimension of the input manifold in the manifold
 472 tracing algorithm.

491 **Manifold tracing algorithm.**

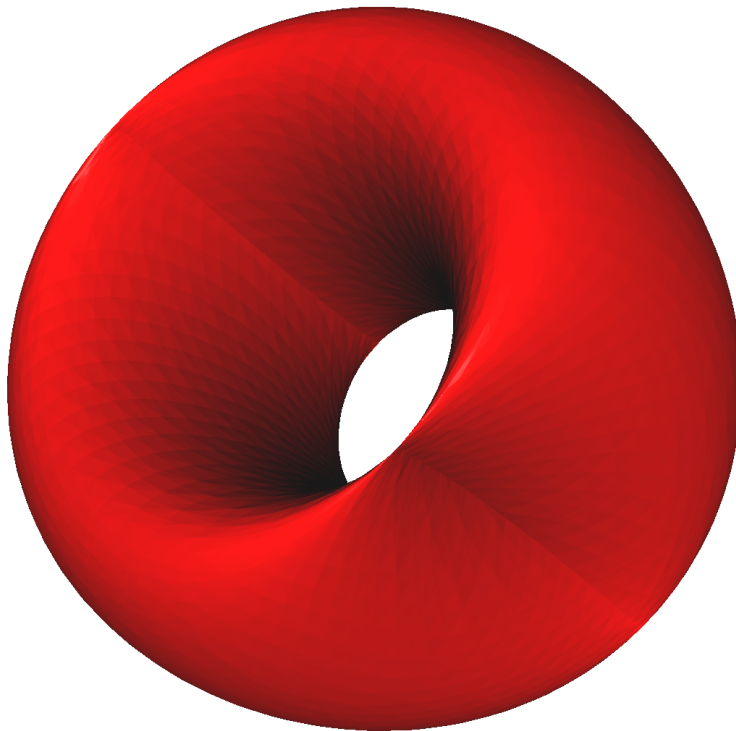
492 We show the performance of our implementation of the manifold tracing algorithm for
 493 various ambient and intrinsic dimensions in Figure 5. In Figure 6, we can see that using
 494 Coxeter triangulation is beneficial in practice as it produces a smaller output in less time. In
 495 Figure 7, we present a PL approximation of a two-dimensional flat torus without boundary
 496 embedded in \mathbb{R}^{10} built by the manifold tracing algorithm. The algorithm can be easily
 497 adapted to handle submanifolds with boundary. In Figure 8, we present the mesh obtained
 498 by our algorithm on a portion of a flat torus embedded in \mathbb{R}^4 and cut by a hypersphere.
 499 Both surfaces in Figure 7 and 8 are rotated and translated in their respective ambient spaces
 500 for visualization purposes. Note that there is no C^2 embedding of the flat torus in \mathbb{R}^3 .



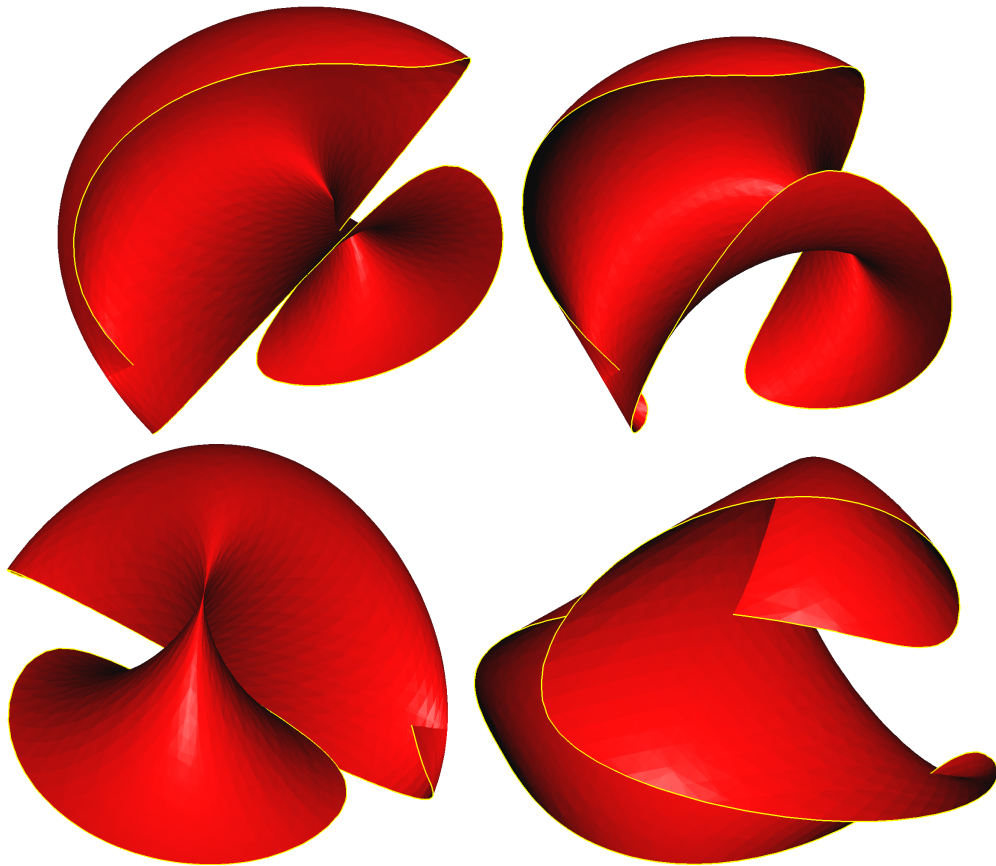
473 **Figure 5** The effect of the ambient dimension d and of the intrinsic dimension m on the compu-
 474 tation time of the of the manifold tracing algorithm. The reconstructed manifold in the tests is the
 475 m -dimensional sphere embedded in \mathbb{R}^d . The ambient triangulation used is a Coxeter triangulation
 476 of type \tilde{A}_d . The diameter of the full simplices is fixed for all d .



477 **Figure 6** Comparison of the size of the output of the manifold tracing algorithm using two types
 478 of the ambient triangulation: a Coxeter triangulation of type \tilde{A}_d (in blue) and the Freudenthal-
 479 Kuhn triangulation of \mathbb{R}^d (in red) with the same diameter $0.07\sqrt{d}$ of d -dimensional simplices. The
 480 reconstructed manifold is the 2-dimensional implicit surface “Chair” embedded in \mathbb{R}^d given by the
 481 equations: $(x_1^2 + x_2^2 + x_3^2 - 0.8)^2 - 0.4((x_3 - 1)^2 - 2x_1^2)((x_3 + 1)^2 - 2x_2^2) = 0$ and $x_i = 0$ for $i > 3$.



482 ■ **Figure 7** The piecewise-linear approximation of a flat torus embedded in \mathbb{R}^{10} defined by the
483 equations $x_1^2 + x_2^2 = 1$ and $x_3^2 + x_4^2 = 1$ and $x_i = 0$ for $i > 4$, projected to \mathbb{R}^3 . The ambient
484 triangulation used is a Coxeter triangulation of type \tilde{A}_{10} with the diameter of the full-dimensional
485 simplices 0.23. The output size $|\mathcal{S}|$ is 509952. The execution time of the algorithm is 231s.



486 ■ **Figure 8** Four views of the flat torus in \mathbb{R}^4 given by two equations $x_1^2 + x_2^2 = 1$ and $x_3^2 + x_4^2 = 1$ cut
487 by the hypersphere $(x_1 - 1)^2 + x_2^2 + (x_3 - 1)^2 + x_4^2 = 4$, projected to \mathbb{R}^3 . The ambient triangulation used
488 is a Coxeter triangulation of type \tilde{A}_4 with the diameter 0.15 of the full-dimensional simplices. The
489 reconstructed boundary is highlighted in yellow. The size $|\mathcal{S}|$ of the piecewise-linear approximation
490 is 14779. The execution time of the algorithm is 1.84s.

501 ——— **References** ———

- 502 **1** Eugene Allgower and Kurt Georg. *Numerical continuation methods: an introduction*,
503 volume 13. Springer Science & Business Media, 1990.
- 504 **2** Eugene Allgower and Phillip H. Schmidt. An algorithm for piecewise-linear approximation
505 of an implicitly defined manifold. *SIAM journal on numerical analysis*, 22(2):322–346,
506 1985.
- 507 **3** Luigi Ambrosio and Halil Mete Soner. Level set approach to mean curvature flow in
508 arbitrary codimension. *J. Differential Geom.*, 43(4):693–737, 1996. URL: <https://doi.org/10.4310/jdg/1214458529>, doi:10.4310/jdg/1214458529.
- 509 **4** M. A. Armstrong. *Groups and Symmetry*. Springer, 1988.
- 510 **5** Praveen Bhaniramka, Rephael Wenger, and Roger Crawfis. Isosurfacing in higher dimen-
511 sions. In *Proceedings of the conference on Visualization'00*, pages 267–273. IEEE Computer
512 Society Press, 2000.
- 513 **6** Jean-Daniel Boissonnat and Arijit Ghosh. Manifold reconstruction using tangential
514 Delaunay complexes. *Discrete & Computational Geometry*, 51(1):221–267, 2014.
- 515 **7** Jean-Daniel Boissonnat, Leonidas J. Guibas, and Steve Oudot. Manifold reconstruction
516 in arbitrary dimensions using witness complexes. *Discrete & Computational Geometry*,
517 42(1):37–70, 2009. URL: <https://doi.org/10.1007/s00454-009-9175-1>, doi:10.1007/
518 s00454-009-9175-1.
- 519 **8** Jean-Daniel Boissonnat, Siargey Kachanovich, and Mathijs Wintraecken. Triangulating
520 submanifolds: An elementary and quantified version of Whitney’s method. Preprint,
521 December 2018. URL: <https://hal.inria.fr/hal-01950149>.
- 522 **9** Jean-Daniel Boissonnat, Siargey Kachanovich, and Mathijs Wintraecken. Tracing isoman-
523 ifolds of arbitrary dimension and codimension. In preparation, December 2019.
- 524 **10** Jean-Daniel Boissonnat and Mathijs Wintraecken. The topological correctness of PL-
525 approximations of isomanifolds. Preprint, November 2019. URL: <https://hal.inria.fr/hal-02386193>.
- 526 **11** Nicolas Bourbaki. Lie groups and Lie algebras. Chapters 4–6. Translated from the 1968
527 French original by Andrew Pressley. *Elements of Mathematics*, 2002.
- 528 **12** S. S. Cairns. On the triangulation of regular loci. *Annals of Mathematics. Second Series*,
529 35(3):579–587, 1934. doi:10.2307/1968752.
- 530 **13** S-W. Cheng, T. K. Dey, and E. A. Ramos. Manifold Reconstruction from Point Samples.
531 In *Proc. ACM-SIAM Symp. Discrete Algorithms*, pages 1018–1027, 2005.
- 532 **14** Siu-Wing Cheng, Tamal K. Dey, and Jonathan Richard Shewchuk. *Delaunay Mesh Gen-
533 eration*. Chapman and Hall / CRC computer and information science series. CRC Press,
534 2013. URL: <http://www.crcpress.com/product/isbn/9781584887300>.
- 535 **15** Aruni Choudhary, Siargey Kachanovich, and Mathijs Wintraecken. Coxeter triangula-
536 tions have good quality. Submitted, December 2017. URL: <https://hal.inria.fr/hal-01667404>.
- 537 **16** Kenneth L. Clarkson. Tighter bounds for random projections of manifolds. In *Proceedings
538 of the 24th ACM Symposium on Computational Geometry, College Park, MD, USA, June
539 9-11, 2008*, pages 39–48, 2008. URL: <https://doi.org/10.1145/1377676.1377685>, doi:
540 10.1145/1377676.1377685.
- 541 **17** J. H. Conway and N. J. A. Sloane. *Sphere-packings, Lattices, and Groups*. Springer-Verlag
542 New York, Inc., New York, NY, USA, 1987.
- 543 **18** Harold S. M. Coxeter. Discrete groups generated by reflections. *Annals of Mathematics*,
544 pages 588–621, 1934.
- 545 **19** Wolfgang A. Dahmen and Charles A. Micchelli. On the linear independence of multivariate
546 B-splines, I. Triangulations of simploids. *SIAM Journal on Numerical Analysis*, 19(5):993–
547 1012, 1982.

- 551 20 Persi Diaconis, Susan Holmesand, and Mehrdad Shahshahani. Sampling from a manifold.
552 *IMS Collections*, 2012.
- 553 21 David P. Dobkin, Allan R. Wilks, Silvio V. F. Levy, and William P. Thurston. Con-
554 tour tracing by piecewise linear approximations. *ACM Transactions on Graphics (TOG)*,
555 9(4):389–423, 1990.
- 556 22 B. Curtis Eaves. *A course in triangulations for solving equations with deformations*, volume
557 234. Lecture Notes in Economics and Mathematical Systems, 1984.
- 558 23 Armin Eftekhari and Michael B. Wakin. What happens to a manifold under a bi-lipschitz
559 map? *Discrete & Computational Geometry*, 57(3):641–673, 2017. URL: <https://doi.org/10.1007/s00454-016-9847-6>, doi:10.1007/s00454-016-9847-6.
- 561 24 Gideon Ehrlich. Loopless algorithms for generating permutations, combinations, and other
562 combinatorial configurations. *Journal of the ACM (JACM)*, 20(3):500–513, 1973.
- 563 25 Hans Freudenthal. Simplicialzerlegungen von beschränkter flachheit. *Annals of Mathemat-*
564 *ics*, pages 580–582, 1942.
- 565 26 Alfred Gray. Comparison theorems for the volumes of tubes as generalizations of the weyl
566 tube formula. *Topology*, 21(2):201–228, 1982.
- 567 27 GUDHI Project. GUDHI Editorial Board. URL: <http://gudhi.gforge.inria.fr/doc/latest/>.
- 569 28 George Haller and Sten Ponsioen. Nonlinear normal modes and spectral submanifolds:
570 existence, uniqueness and use in model reduction. *Nonlinear dynamics*, 86(3):1493–1534,
571 2016.
- 572 29 James E. Humphreys. *Reflection groups and Coxeter groups*, volume 29. Cambridge uni-
573 versity press, 1992.
- 574 30 Siargey Kachanovich. *Manifold meshing using Coxeter triangulations*. PhD thesis, Uni-
575 versité Côte d’Azur, 2019.
- 576 31 S. M. LaValle. *Planning Algorithms*. Cambridge University Press, Cambridge, U.K., 2006.
577 Available at <http://planning.cs.uiuc.edu/>.
- 578 32 William E. Lorensen and Harvey E. Cline. Marching cubes: A high resolution 3d surface
579 construction algorithm. In *ACM siggraph computer graphics*, volume 21, pages 163–169.
580 ACM, 1987.
- 581 33 M. Maes and B. Kappen. On the permutahedron and the quadratic placement problem.
582 *Philips Journal of Research*, 46(6):267–292, 1992.
- 583 34 Shawn Martin, Aidan Thompson, Evangelos A Coutsias, and Jean-Paul Watson. Topology
584 of cyclo-octane energy landscape. *The journal of chemical physics*, 132(23):234115, 2010.
- 585 35 Chohong Min. Simplicial isosurfacing in arbitrary dimension and codimension. *Journal of*
586 *Computational Physics*, 190(1):295–310, 2003.
- 587 36 Hariharan Narayanan and Partha Niyogi. Sampling hypersurfaces through diffusion. In
588 *12th Intl. Workshop on Randomization and Computation (RANDOM)*, 2008.
- 589 37 B.C. Rennie and A.J. Dobson. On Stirling numbers of the second kind. *Journal of Combin-*
590 *atorial Theory*, 7(2):116 – 121, 1969. URL: [http://www.sciencedirect.com/science/](http://www.sciencedirect.com/science/article/pii/S0021980069800451)
591 [article/pii/S0021980069800451](http://www.sciencedirect.com/science/article/pii/S0021980069800451), doi:[https://doi.org/10.1016/S0021-9800\(69\)](https://doi.org/10.1016/S0021-9800(69)80045-1)
592 [80045-1](https://doi.org/10.1016/S0021-9800(69)80045-1).
- 593 38 Frank Ruskey and Carla D. Savage. Gray codes for set partitions and restricted growth
594 tails. *Australasian J. Combinatorics*, 10:85–96, 1994.
- 595 39 Michael J. Todd. *The computation of fixed points and applications*, volume 124. Lecture
596 Notes in Economics and Mathematical Systems, 1976.
- 597 40 Nakul Verma. A note on random projections for preserving paths on a manifold. Technical
598 Report Tech. Report CS2011-0971, UC San Diego, 2011.
- 599 41 Timothy R. Walsh. Loop-free sequencing of bounded integer compositions. *Journal of*
600 *Combinatorial Mathematics and Combinatorial Computing*, 33:323–345, 2000.

601 42 Rephael Wenger. *Isosurfaces: geometry, topology, and algorithms*. AK Peters/CRC Press, 2013.
 602
 603 43 Hermann Weyl. On the volume of tubes. *American Journal of Mathematics*, 61(2):461–472, 1939.
 604
 605 44 J. H. C. Whitehead. On C^1 -complexes. *Annals of Mathematics*, 41(4):809–824, 1940. URL: <http://www.jstor.org/stable/1968861>.
 606
 607 45 H. Whitney. *Geometric Integration Theory*. Princeton University Press, 1957.
 608 46 G. M. Ziegler. *Lectures on Polytopes*. Graduate Texts in Mathematics. Springer New York, 2012. URL: <https://books.google.fr/books?id=xd25TXSSUcgC>.
 609

610 **A Proofs for Section 2.4**

611 In this appendix we will prove that the Freudenthal-Kuhn triangulation is the Coxeter
 612 triangulations of type \tilde{A}_d up to a linear transformation. We also prove that the Voronoi cell
 613 of a vertex in a Coxeter triangulation of type \tilde{A}_d is a permutahedron.

614 For this we need to first recall an equivalent definition of the Coxeter triangulations of
 615 type \tilde{A}_d : Any Coxeter triangulation can be defined as an hyperplane arrangement

616
$$\mathcal{H} = \{H_{r,k} \mid r \in R_+, k \in \mathbb{Z}\},$$

617 where

618
$$H_{u,k} = \{x \in \mathbb{R}^d \mid \langle x, u \rangle = k\},$$

619 and R_+ denotes the set of *positive roots* of the Coxeter group. We will not recall the general
 620 definition of positive roots, which can be found in for example [11, 29, 15], but use that for
 621 \tilde{A}_d , according to [11, Planche II],

622
$$R_+ = \left\{ r_{i,j} = \sum_{l=i}^j s_l \mid 1 \leq i \leq j \leq d \right\},$$

623 with $\{s_i\}$ the *simple roots* of the Weyl group A_d associated to the triangulation of type \tilde{A}_d .
 624 For a discussion of the Weyl group we again refer to for example [11, 29, 15]. We also recall
 625 the simple roots of A_d , which will be needed in the second proof. The simple roots of A_d
 626 (in the hyperplane $P = \{(x^i) \in \mathbb{R}^{d+1} \mid \sum_i x^i = 0\} \subset \mathbb{R}^{d+1}$) are in turn:

627
$$s_1 = e_1 - e_2, s_2 = e_2 - e_3, \dots, s_d = e_d - e_{d+1},$$

628 see [11]. We stress that these simple roots can be rescaled, permuted and rotated in
 629 the hyperplane P . We note that one can easily rotate $\mathbb{R}^d \subset \mathbb{R}^{d+1}$ given by the first d
 630 basis vectors into P . The matrix in $\text{SO}(d+1)$ of this transformation has as first d rows
 631 $((1/\sqrt{i^2+i})^{\{i\}}, -i/\sqrt{i^2+i}, 0^{\{d-i-1\}})$ and the final row $((1/\sqrt{d+1})^{\{d+1\}})$, where $c^{\{k\}}$ de-
 632 notes k consecutive coordinates equal to c . We will not use this transformation because it
 633 complicates the expressions prohibitively.

634 In Lemma 9, we have seen that $x \in \mathbb{R}^d$ lies on the face of some simplex with canonical
 635 permutahedral representation (\tilde{v}_0, ω) in the FK-triangulation if and only if either $x^i - \tilde{v}_0^i =$
 636 $x^j - \tilde{v}_0^j$ or $x^i - \tilde{v}_0^i = 0$ for some i, j . Note that $\tilde{v}_0^i, \tilde{v}_0^j \in \mathbb{Z}$. Hence we see that

637 **► Lemma 27.** *The Freudenthal-Kuhn triangulation is a hyperplane arrangement $\tilde{\mathcal{H}} = \{H_{u,k} \mid$
 638 $u \in E, k \in \mathbb{Z}\}$, with*

639
$$E = \{e_1, \dots, e_d\} \cup \{u_{i,j} = e_j - e_i \mid 1 \leq i < j \leq d\}.$$

640 We now define a linear map μ from \mathbb{R}^d to P by showing how it acts on the basis:

$$641 \quad \mu(e_i) = r_{1,i} = \sum_{i=1}^j s_i.$$

642 We claim that μ maps E bijectively onto R_+ . The vector $\mu(e_i) = r_{1,i}$ lies in R_+ , by
643 construction. For $u_{i,j} \in E$, with $i < j$, we see that

$$644 \quad \mu(u_{i,j}) = \mu(e_j - e_i) = \mu(e_j) - \mu(e_i) = r_{1,j} - r_{1,i} = \sum_{l=1}^j s_l - \sum_{l=1}^i s_l = \sum_{l=i+1}^j s_l = r_{i+1,j}.$$

645 Hence $\mu(u_{i,j})$ lies in R_+ . By reading the previous calculation backwards we see that μ^{-1}
646 maps each $r \in R_+$ to a vector in E .

647 We conclude that μ (bijectively) maps \mathcal{H} to $\tilde{\mathcal{H}}$, which completes the proof of Lemma 19.
648

649 We now prove the following:

650 ► **Proposition 28.** *The Voronoi cell of a Coxeter triangulation of type \tilde{A}_d is a permutahed-*
651 *ron.*

652 **Proof.** We start by recalling a number of results. In [15] we have seen that the circumcentre
653 of the simplex given in Definition 18 is

$$654 \quad c = \left(-\frac{d-2i}{2(d+1)} \right),$$

655 with $i \in \{0, \dots, d\}$. The circumcentre of a Delaunay simplex is a Voronoi vertex. We recall
656 that

- 657 ■ All simplices in the star of 0 in the Coxeter triangulation are found by consecutive
658 reflection of the simplex of Definition 18 in the hyperplanes of \mathcal{H} that go through 0, that
659 is the hyperplanes with normals $r_{j,k} = e_j - e_k$, with $j \neq k$. See for example [11, 29, 15].
660 We also call these reflections the action of the Weyl group.

- 661 ■ The reflection $R_{j,k}$ in a plane that goes through the origin with normal $r_{j,k}$ is given by

$$662 \quad R_{j,k}(v) = v - 2 \frac{v \cdot r_{j,k}}{r_{j,k} \cdot r_{j,k}} r_{j,k} = v - (v \cdot r_{j,k}) r_{j,k}.$$

663 We find that

$$664 \quad R_{j,k}(c)^i = (c - (c \cdot r_{j,k}) r_{j,k})^i = -\frac{d-2i}{2(d+1)} - \frac{2j-2k}{2(d+1)} (\delta_{ij} - \delta_{ik}),$$

665 which permutes the j th and k th coordinate of c . Here we used the upper index i to denote
666 the i th coordinate. Using the cycle notation for the permutation group, see for example [4,
667 Chapter 6], this coincides the 2-cycle (jk) . Let now

$$668 \quad c_\pi = \left(-\frac{d-2\pi_i}{2(d+1)} \right),$$

669 with $\{\pi_i\}$ some permutation of $\{0, \dots, d\}$. We find that

$$670 \quad R_{j,k}(c_\pi)^i = (c_\pi - (c_\pi \cdot r_{j,k}) r_{j,k})^i = -\frac{d-2\pi_i}{2(d+1)} - \frac{2\pi_j-2\pi_k}{2(d+1)} (\delta_{ij} - \delta_{ik}),$$

671 which again permutes the j th and k th coordinate. Now recall that all permutations are
672 generated by 2-cycles, see for example [4, Theorem 6.1]. This implies that, for any permuta-
673 tion π , we can find c_π from c by the action of the Weyl group. This also means that we
674 have explicitly described the Voronoi cell of 0 in the Coxeter triangulation of type \tilde{A}_d as a
675 permutahedron. Because of symmetry, this now holds for any Voronoi cell. ◀

676 **B Proofs for Section 2.1**

677 The proof of Corollary 6 is based on:

678 ▶ **Lemma 29** (Lemma 3.11 of [33]). *The face of a permutahedron corresponding to an ordered*
 679 *partition $\omega = (\omega_1, \dots, \omega_{l+1})$ is combinatorially*

680
$$\mathcal{P}(|\omega_1|) \times \dots \times \mathcal{P}(|\omega_{l+1}|),$$

681 *where $|\omega_i|$ denotes the length of the i th part of the ordered partition and $\mathcal{P}(k)$ the permuta-*
 682 *hedron of dimension k .*

683 **Proof of Corollary 6.** Since the number of vertices of the product of two polytopes is the
 684 product of the vertices and a k dimensional permutahedron has $(k + 1)!$ vertices, we see
 685 that the total number of vertices of a face of a permutahedron corresponding to an ordered
 686 partition $\omega = (\omega_1, \dots, \omega_{l+1})$ is

687
$$\prod_i (|\omega_i|!).$$

688 Let $1 \leq k < j \leq d$, be integers such that $k + j = d + 1$. By definition $k!j! < (k - 1)!(j + 1)!$,
 689 and thus $k!j! \leq 1!d!$. Generalizing this, we see that the product of the $|\omega_i|!$ is maximal when
 690 all parts are singletons except the biggest part which has $d + 1 - l$ elements. Therefore

691
$$\prod_i (|\omega_i|!) \leq (d - l + 1)!.$$

692 ◀

693 **Proof of Lemma 7.** We first recall a set of $d > 2$ objects can be subdivided in two non-
 694 empty ordered subsets A and B in $2^d - 2$ ways. This is not hard to see. Because we pick for
 695 each element if it will be put in A or B there are 2^d possibilities. Excluding that A or B is
 696 empty gives $2^d - 2$. Let $\omega = (\omega_1, \dots, \omega_l)$ again be an ordered partition. To find a refinement
 697 of ω in $l + 1$ parts we need to first pick a $1 \leq i \leq l$, such that $|\omega_i| > 1$ and then we need to
 698 break ω_i up into two (ordered) parts, for which there are $2^{|\omega_i|} - 2$ possibilities as we have
 699 seen above. This means that if $I = \{i \mid 1 \leq i \leq l, |\omega_i| > 1\}$, the number of refinements is

700
$$\sum_{i \in I} 2^{|\omega_i|} - 2.$$

701 Let now $1 \leq k < j \leq d$ be integers such that $k + j = d + 1$. Then $2^k + 2^j < 2^{k-1} + 2^{j+1}$.
 702 Generalizing this, we see that the sum of the $2^{|\omega_i|} - 2$ is maximal when all $|\omega_i| = 1$ except
 703 the biggest part which has $d - l + 1$ elements. ◀